

Symbolic Learning of Interpretable Reduced-Order Models for Jumping Quadruped Robots

Gioele Buriani[†]* Jingyue Liu[†]* Maximilian Stölzle^{**}
Cosimo Della Santina^{***} Jiatao Ding^{****}

* *Department of Cognitive Robotics, Delft University of Technology, Building 34, Mekelweg 2, 2628 CD Delft, Netherlands (e-mail: gioele.buriani@gmail.com, J.Liu-14@tudelft.nl).*

** *Computer Science and Artificial Intelligence Laboratory (CSAIL), Massachusetts Institute of Technology, Cambridge, MA 02139 USA (e-mail: M.W.Stolzle@tudelft.nl).*

*** *Institute of Robotics and Mechatronics, German Aerospace Center (DLR), 82234 Wessling, Germany (e-mail: C.DellaSantina@tudelft.nl).*

**** *Department of Industrial Engineering, University of Trento (e-mail: jiatao.ding@unitn.it).*

Abstract: Reduced-order models are essential for motion planning and control of quadruped robots, as they simplify complex dynamics while preserving critical behaviors. This paper introduces a novel methodology for deriving such interpretable dynamic models, specifically for jumping. We capture the high-dimensional, nonlinear jumping dynamics in a low-dimensional latent space by proposing a learning architecture combining Sparse Identification of Nonlinear Dynamics (SINDy) with physical structural priors on the jump dynamics. Our approach demonstrates superior accuracy to the traditional actuated Spring-loaded Inverted Pendulum (aSLIP) model and is validated through simulation and hardware experiments across different jumping strategies.

Keywords: Quadruped Robots, Dynamic Modeling, Symbolic Regression, Autoencoders, Interpretability, Reduced-order Models.

1. INTRODUCTION

Recently, quadruped robots have garnered significant attention due to their versatility and potential applications in various fields, including search and rescue missions, agricultural tasks, and exploration in hazardous environments (Gong et al., 2023; Sombolostan and Nguyen, 2024). The performance of these robots depends on accurate dynamic modeling to capture their complex locomotion behaviors.

Traditional modeling techniques, such as the Lagrangian and Newton-Euler methods, have been widely used to derive high-fidelity whole-body dynamic models for quadruped robots (Bellicoso et al., 2017; Di Carlo et al., 2018; Yan et al., 2021; Ding et al., 2024b). However, these high-dimensional models are often computationally intractable for real-time applications due to their complexity (Li et al., 2023). To address this, Researchers have developed reduced-order template models that approximate essential dynamics while significantly lowering computational costs. Examples include the famous Spring-Loaded Inverted Pendulum (SLIP) model (Blickhan, 1989) and the Single Rigid

Body (SRB) (Hong et al., 2020), which simplifies multi-body interactions into low-dimensional representations, enabling efficient analysis of gaits like running and hopping. However, such simplifications often sacrifice accuracy, particularly in scenarios involving multi-contact transitions, nonlinear limb dynamics, or complex terrain interactions (Spröwitz et al., 2013; Carpentier and Mansard, 2018).

To tackle this issue, we investigate the possibility of using a data-driven strategy to learn reduced-order models directly, with a particular interest in the compact, interpretable, and precise description of jumping dynamics, which is very challenging. Numerous studies have utilized machine learning and deep learning methods to model the complex dynamics of various systems (Calandra et al., 2015; Ogunmolu et al., 2016; Rajendra and Brahmajirao, 2020; Hashemi et al., 2023). Dimensionality reduction techniques like autoencoders have been employed to extract low-dimensional features in a latent space (Hinton and Salakhutdinov, 2006; Gonzalez and Balajewicz, 2018; Refinetti and Goldt, 2022), and then Multilayer Perceptrons (MLPs) or Recurrent Neural Networks (RNNs) can learn the dynamics in this low-dimensional space, but at the expense of interpretability in exchange for accuracy. Recent hybrid approaches that combine physics with

¹ This work is supported by the European Union’s Horizon Europe Program Project EMERGE - Grant Agreement No. 101070918.

² [†] These authors contributed equally to this work.

learning (Stölzle, 2025), such as Physics-Informed Neural Networks (PINNs) (Raissi et al., 2019), Deep Lagrangian Networks (DeLaNs) (Lutter et al., 2019; Liu et al., 2024), Coupled Oscillator Networks (CONS) (Stölzle and Santina, 2024), integrate physical laws with deep learning, enhancing accuracy, interpretability, data efficiency, and out-of-distribution performance. However, PINNs often require physics knowledge that is only available to domain experts. Furthermore, nonlinear time-dependent behaviors, as for example experienced during contact phases with the environment, are usually not included in the physical priors and can, therefore, not be learned by the DeLaNs. Symbolic regression, particularly SINDy (Brunton et al., 2016; Pandey et al., 2024), presents an alternative through interpretable symbolic equations, though their application to quadruped robots remains unexplored.

This work proposes a novel methodology to derive reduced-order, interpretable dynamic models for jumping robots. Building upon SINDy autoencoders (Champion et al., 2019), our approach uses a linear³ autoencoder with shared weights to reduce the dimension of the state space while keeping configurations and maintaining their derivatives distinct in the latent space. We map inputs to latent space through the trained autoencoder, optimizing its weights concurrently with the SINDy latent model using an ad-hoc loss function. Considering the hybrid nature of the system during different jumping phases, we learn a consistent model across various hybrid phases by first training the encoder in one phase (e.g., the launching and landing phase), then optimizing the decoder across all phases, and finally learning the SINDy parameters with frozen autoencoder weights.

The main contributions of this work are threefold:

- We present a novel modeling approach that integrates SINDy with a linear autoencoder, utilizing shared weights to derive reduced-order, interpretable models for quadruped robots. This method enhances computational efficiency and model interpretability.
- We propose a sequential training strategy to accurately model the distinct jump phases, ensuring a consistent model across various hybrid phases.
- We evaluate our novel approach on various quadruped robots with different jumping modalities to demonstrate versatility.

The rest of this paper follows: Section 2 covers preliminary concepts; Section 3.1 discusses the proposed learning architecture; Section 3 describes the remaining aspects of our experimental methodology; Section 4 evaluates the method, featuring simulation results for various quadruped models, latent dimensionality analysis, and hardware validation. Section 5 concludes this work.

2. PRELIMINARY

Traditional modeling approaches, such as multi-rigid-body dynamics, represent quadruped robots as a movable base (i.e., the body) with kinematic chains (i.e., the legs) at-

³ The linearity of the autoencoder is critical for preserving interpretability and facilitating the closed-form, analytical (i.e., without autodifferentiation) computation of time derivatives.

tached, applicable to various quadruped robots, as shown in Fig. 1.

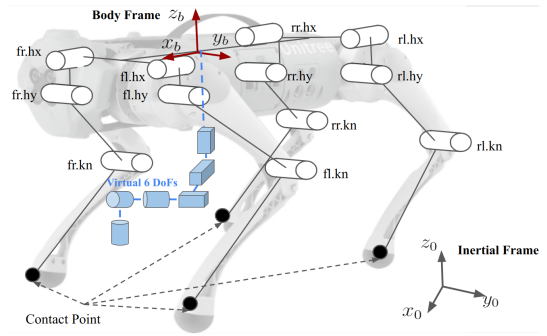


Fig. 1. Quadruped robot with labeled joints and body frame.

As illustrated in Fig. 1, the Unitree Go1, for example, exhibits 12 Degrees of Freedom (DOFs) for the limbs alone, with 6 underactuated DoFs for the floating base’s position and orientation relative to an inertial frame (Righetti et al., 2011).

The configuration space of quadruped robots is typically parameterized as (Mistry et al., 2010)

$$\mathbf{q} = [\mathbf{q}_j^\top \mathbf{q}_b^\top]^\top \in \mathbb{R}^{m+6}, \quad (1)$$

where $\mathbf{q}_j \in \mathbb{R}^m$ contains the coordinates of the actuated joints, with m representing the number of joints, and $\mathbf{q}_b \in SE(3)$ captures the coordinates of the unactuated floating base, including Cartesian positions $(x, y, z) \in \mathbb{R}^3$ and Euler angles $(\phi, \theta, \psi) \in SO(3)$. The constrained dynamics follow

$$\mathbf{M}(\mathbf{q}) \ddot{\mathbf{q}} + \mathbf{h}(\mathbf{q}, \dot{\mathbf{q}}) = \mathbf{S}^\top \boldsymbol{\tau} + \mathbf{J}_c^\top(\mathbf{q}) \boldsymbol{\lambda}, \quad (2)$$

where $\mathbf{M}(\mathbf{q}) \in \mathbb{R}^{(m+6) \times (m+6)}$ is the mass matrix, $\mathbf{h}(\mathbf{q}, \dot{\mathbf{q}}) \in \mathbb{R}^{m+6}$ captures centripetal, Coriolis, and gravitational forces, $\mathbf{S} = [\mathbf{I}_{m \times m} \mathbf{0}_{m \times 6}]$ is the selection matrix for actuated joints, $\boldsymbol{\tau} \in \mathbb{R}^m$ denotes actuation torques, $\mathbf{J}_c \in \mathbb{R}^{k \times (m+6)}$ is the Jacobian matrix for k linearly independent constraints, and $\boldsymbol{\lambda} \in \mathbb{R}^k$ represents the constraint forces.

Consider a quadruped robot where ground reaction forces (GRFs) constitute the dominant constraint forces acting on the body. For each leg (modeled as an independent kinematic chain), the GRF $\mathbf{F}_k \in \mathbb{R}^3$ at the k -th foot can be computed from the joint torques $\boldsymbol{\tau}_k$ through the leg Jacobian transpose

$$\mathbf{F}_k = \mathbf{J}_k^{-\top} \boldsymbol{\tau}_k, \quad (3)$$

where $\mathbf{J}_k \in \mathbb{R}^{3 \times n_j}$ is the Jacobian of the k -th leg ($n_j = m/4$ being the number of joints per leg).

The net effect of GRFs on the robot’s center of mass (CoM) dynamics can be described by the time derivatives of the linear and angular momentum of the CoM

$$\dot{\mathcal{P}} = \sum_{k=1}^4 \mathbf{F}_k, \quad \dot{\mathcal{L}} = \sum_{k=1}^4 ((\mathbf{p}_k - \mathbf{b}) \times \mathbf{F}_k), \quad (4)$$

where $\mathcal{P} \in \mathbb{R}^3$ and $\mathcal{L} \in \mathbb{R}^3$ are the linear and angular momentum, respectively. Here, $\mathbf{p}_k \in \mathbb{R}^3$ denotes the world-frame position of the k -th leg, and $\mathbf{b} \in \mathbb{R}^3$ is the CoM position in world coordinates.

The generalized wrench $\mathcal{F} \in \mathbb{R}^6$ that acts on the body frame is

$$\mathcal{F} = \begin{bmatrix} \dot{\mathbf{p}}^\top & \dot{\mathbf{l}}^\top \end{bmatrix}^\top \in \mathbb{R}^6, \quad (5)$$

which leads to the complete system input formulation

$$\mathbf{u} = \begin{bmatrix} \boldsymbol{\tau}^\top & \mathcal{F}^\top \end{bmatrix}^\top \in \mathbb{R}^{m+6}. \quad (6)$$

3. METHODOLOGY

3.1 Proposed Learning Architecture

We present a novel framework combining linear autoencoders with SINDy to model quadruped dynamics, incorporating physical priors for dimensionality reduction while preserving essential dynamic features. Our approach achieves dimensionality reduction while preserving the essential dynamic characteristics, enabling efficient representation of complex jumping motions

Fig. 2 provides an overview of the encoded latent space and the established dynamics loop.

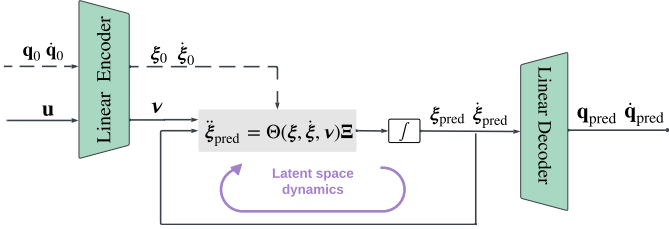


Fig. 2. Overview of our proposed methodology: We learn symbolic reduced-order dynamics $\ddot{\xi} = \Theta(\xi, \dot{\xi}, \nu)\Xi$ that operate in a low-dimensional space $(\xi, \dot{\xi})$. This allows us to predict the time evolution of the higher-dimensional system states $(\mathbf{q}, \dot{\mathbf{q}})$. Here, \mathbf{q}_0 and $\dot{\mathbf{q}}_0$ represent the initial state.

Fig. 3 details the training process, including the encoder-decoder structure, latent space dynamics prediction, and real-space dynamics reconstruction. The algorithm includes encoding the initial state into a latent space, predicting dynamics in this latent space, and decoding them back to the full-order system space. We ensure accurate reconstruction of system states and dynamical modeling through specialized loss components.

The linear autoencoder is designed to reduce the dimensionality of the state space while preserving a clear linear relationship with the original space, thereby maintaining direct interpretability. The autoencoder consists of an encoder $(\mathbf{W}_e, \mathbf{B}_e)$ and a decoder $(\mathbf{W}_d, \mathbf{B}_d)$. The encoder's weights and bias are $\mathbf{W}_e \in \mathbb{R}^{l \times (m+6)}$ and $\mathbf{B}_e \in \mathbb{R}^l$, while the decoder's weights and bias are $\mathbf{W}_d \in \mathbb{R}^{(m+6) \times l}$ and $\mathbf{B}_d \in \mathbb{R}^{m+6}$, where l is the dimension of the desired latent space configuration.

The encoder maps the robot's configuration \mathbf{q} and its derivatives $\mathbf{q}^{(n)}$ into a lower-dimensional latent space using the linear transformation

$$\boldsymbol{\xi}^{(n)} = \mathbf{W}_e \mathbf{q}^{(n)} + \delta_{n0} \mathbf{B}_e, \quad n = 0, 1, 2, \quad (7)$$

where $\boldsymbol{\xi} \in \mathbb{R}^l$ represents the latent representation, $\boldsymbol{\xi}^{(n)}$ denotes the n -th derivative of $\boldsymbol{\xi}$, and δ_{n0} is the Kronecker delta, equal to 1 when $n = 0$ and 0 otherwise. The system's actuation is mapped into latent space as

$$\boldsymbol{\nu} = \mathbf{W}_e^{-\top} \mathbf{u} \in \mathbb{R}^l. \quad (8)$$

After establishing the latent space mapping, we employ the SINDy algorithm (Brunton et al., 2016) to identify symbolic representations of the latent dynamics (see Fig. 3b). SINDy constructs a symbolic library of candidate functions $\Theta(\boldsymbol{\xi}, \dot{\boldsymbol{\xi}}, \boldsymbol{\nu})$, including polynomial and trigonometric functions of latent variables $(\boldsymbol{\xi})$, their derivatives $(\boldsymbol{\xi}^{(n)})$, and the transformed control inputs $(\boldsymbol{\nu})$. This library represents a comprehensive set of terms that might appear in the system's governing equations. The objective is to represent the dynamics of the latent variables as a sparse combination of these candidate functions. Mathematically, this is expressed as a sparse regression problem, with the latent dynamics expressed as

$$\ddot{\boldsymbol{\xi}}_{\text{pred}} = \Theta(\boldsymbol{\xi}, \dot{\boldsymbol{\xi}}, \boldsymbol{\nu}) \boldsymbol{\Xi}, \quad (9)$$

where $\boldsymbol{\Xi} \in \mathbb{R}^{p \times l}$ is a sparse matrix of coefficients to be determined, with p being the number of the candidate functions in $\Theta(\boldsymbol{\xi}, \dot{\boldsymbol{\xi}}, \boldsymbol{\nu})$. The optimization problem is typically solved using sequential thresholding methods to ensure a sparse solution (Brunton et al., 2016; Champion et al., 2019). Promotes sparsity by penalizing the ℓ_1 -norm of $\boldsymbol{\Xi}$, which encourages most entries in $\boldsymbol{\Xi}$ to be zero. This sparsity-promoting optimization ensures that only a minimal set of candidate functions is selected, resulting in an interpretable and computationally efficient model.

Subsequently, the predicted accelerations in the latent space, $\ddot{\boldsymbol{\xi}}_{\text{pred}}$, are transformed back to the original state space by the linear decoder

$$\ddot{\mathbf{q}}_{\text{pred}} = \mathbf{W}_d \ddot{\boldsymbol{\xi}}_{\text{pred}}. \quad (10)$$

For training encoder, decoder, and reduced-order symbolic dynamics, we consider the following loss components:

- $\mathcal{L}_{\text{recon}} = \|\mathbf{q} - \mathbf{q}_{\text{recon}}\|_2^2$ ensures accurate reconstruction of the original state. The reconstructed configuration $\mathbf{q}_{\text{recon}}$ is given by
- $$\mathbf{q}_{\text{recon}} = \mathbf{W}_d (\mathbf{W}_e \mathbf{q} + \mathbf{B}_e) + \mathbf{B}_d. \quad (11)$$
- $\mathcal{L}_{\text{SINDy}} = \|\ddot{\boldsymbol{\xi}} - \ddot{\boldsymbol{\xi}}_{\text{pred}}\|_2^2 + \|\ddot{\mathbf{q}} - \ddot{\mathbf{q}}_{\text{pred}}\|_2^2$ captures the prediction loss, ensuring that the learned dynamics in the latent space and the reconstructed space are accurate.
 - $\mathcal{L}_{\text{reg}} = \|\boldsymbol{\Xi}\|_1$ promotes sparsity in SINDy coefficients.

3.2 Training with Multi-Phase Motions

Jumping motion poses unique modeling challenges due to its hybrid dynamical nature. This study considers two types of jumping: the synchronized and the froggy jumps.

In the synchronized jump, the robot launches and lands with full limb contact simultaneously. This motion consists of two dominant phases: (1) a contact phase, where all legs remain grounded during takeoff and landing, and (2) a flight phase, where the robot is entirely airborne.

Conversely, the froggy jump consists of an initial phase where all legs are grounded, followed by a transition phase where only the rear legs remain in contact with the ground, and then progressing to a flight phase.

To effectively model the hybrid jumping dynamics, we propose a structured training methodology (Fig. 3) that combines transfer learning principles (Torrey and Shavlik, 2010) with phase-specific optimization. First, we train

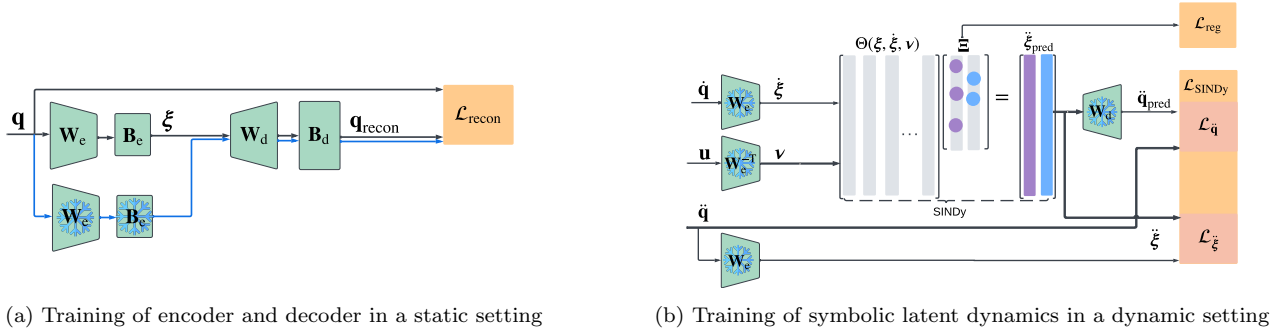


Fig. 3. Detailed visualization of the training methodology. **(a)**: The linear autoencoder is first trained on the contact phase dataset, minimizing the reconstruction loss, \mathcal{L}_{rec} , depicted by the black line. Subsequently, in the second step (visualized with a blue line in the flowchart), the encoder weights are kept fixed, and the decoder is fine-tuned on a dataset that includes all motion phases. **(b)**: In the third step, we train, for each motion phase separately, a symbolic dynamical model $\ddot{\xi}_{\text{pred}}$ in latent space. Here, we employ the SINDy approach to regress a sparse matrix Ξ that selects and scales basis functions from the library $\Theta(\xi, \dot{\xi}, \nu)$. The loss components $\mathcal{L}_{\text{SINDy}}$ and \mathcal{L}_{reg} ensure accurate dynamics prediction and sparsity of the coefficients, respectively. The SINDy loss $\mathcal{L}_{\text{SINDy}}$ is calculated based on the predicted reduced-order model accelerations, $\ddot{\xi}_{\text{pred}}$, and the corresponding decoded configuration-space accelerations, $\ddot{\mathbf{q}}_{\text{pred}}$. Importantly, we keep the autoencoder weights frozen, which preserves training stability and ensures that the reconstructions remain accurate during all motion phases.

the encoder and decoder statically on reconstructing the configurations of the full contact phase by minimizing the $\mathcal{L}_{\text{recon}}$ loss. Then, the encoder weights are frozen, and the decoder is trained on all motion phases, including the flight phase, still minimizing $\mathcal{L}_{\text{recon}}$. Finally, with the encoder and decoder weights fixed, we train the symbolic dynamics for each motion phase (contact, partial contact, and flight) by minimizing the $\mathcal{L}_{\text{SINDy}}$ and \mathcal{L}_{reg} loss terms, efficiently capturing the hybrid nature of the jumping dynamics.

This training methodology ensures that the final model is physically coherent and can accurately reconstruct the robot’s motion across different phases. By leveraging transfer learning, we create robust models that effectively capture hybrid dynamics, enhance interpretability, and seamlessly handle complex, phase-dependent behaviors.

3.3 Data Collection and Preprocessing

Datasets were collected from both simulated and real-world environment. Simulated data were generated using the PyBullet engine (Coumans and Bai, 2016) with Unitree Go1 and A1 robots. Real-world data were gathered from an actual Go1 robot to validate the simulation results, ensure practical applicability, and benchmark the algorithm’s performance on real-world, noisy data.

Simulation data for the Go1 quadruped robot captured forward jumping motions, as shown in Fig. 4a, achieved with Model Predictive Control (MPC) (Ding et al., 2024a). Additionally, data from the Unitree A1 quadruped for froggy jumping behavior, as visualized in Fig. 4b, were collected using a Cartesian PD controller (Nguyen and Nguyen, 2022). For both robots, the dataset includes joint angles and velocities ($\mathbf{q}_j, \dot{\mathbf{q}}_j \in \mathbb{R}^{12}$), body position and velocity ($\mathbf{q}_b, \dot{\mathbf{q}}_b \in \mathbb{R}^6$), input torques ($\boldsymbol{\tau} \in \mathbb{R}^{12}$), and the contact state ($\mathbf{c} \in \mathbb{R}^4$) for each timestep.

The Go1 simulated data consists of 156 jumps (120 for training, 30 for validation, and 6 for testing), with each jump having 800 data points: 300 for launching, 300 for

landing (totaling 600 contact points), and 200 for flight. The A1 simulated dataset contains 150 jumps (100 for training, 40 for validation, and 10 for testing), with each jump comprising 1200 data points: 400 for launch, 400 for landing (800 contact points), and 400 for flight. To enhance robustness, a variant of the datasets with added noise as described in the work from Ding et al. (2024a).

Real-world data were collected from a Go1 quadruped, as depicted in Fig. 4c. The quadruped was operated using the same control algorithm as in the simulation, with data collection performed similarly using the official Go1 SDK. This dataset comprises 15 jumps, distributed as 12 for training, 2 for validation, and 1 for testing, maintaining the same data point distribution as the Go1 simulated data.

The collected data are preprocessed to compute necessary derivatives and forces. The state’s acceleration $\ddot{\mathbf{q}}$ is calculated by numerically differentiating the velocity data $\dot{\mathbf{q}}$. The force on the CoM, $\mathcal{F} \in \mathbb{R}^6$, is calculated based on Eq. 4 and 5, forming the final system input, \mathbf{u} .

3.4 Evaluation Procedure

To validate the final model Θ , a single dataset is selected from multiple test jumps. The initial system state ($\mathbf{q}_0, \dot{\mathbf{q}}_0$) and inputs \mathbf{u} are transformed by the trained encoder and the input transformation equation to the latent initial state ($\xi_0, \dot{\xi}_0$) and ν , respectively. The model then predicts latent configuration accelerations $\ddot{\xi}_{\text{pred}}$, which are integrated using the *lsoda* method (Hindmarsh and Petzold, 2005) to obtain predicted latent space state ξ_{pred} and $\dot{\xi}_{\text{pred}}$ with a step size of 500 Hz. This process is repeated for each time step. The predicted latent configuration ξ_{pred} is then decoded into a real space configuration by $\mathbf{q}_{\text{pred}} = \mathbf{W}_d \xi_{\text{pred}} + \mathbf{B}_d$ for direct comparison with actual jump data. An alternative evaluation approach involves simulating the learned system for shorter intervals (e.g., 0.1 s – 50 steps) with periodic resets to the original latent state ($\xi, \dot{\xi}$). This strategy decreases error accumula-

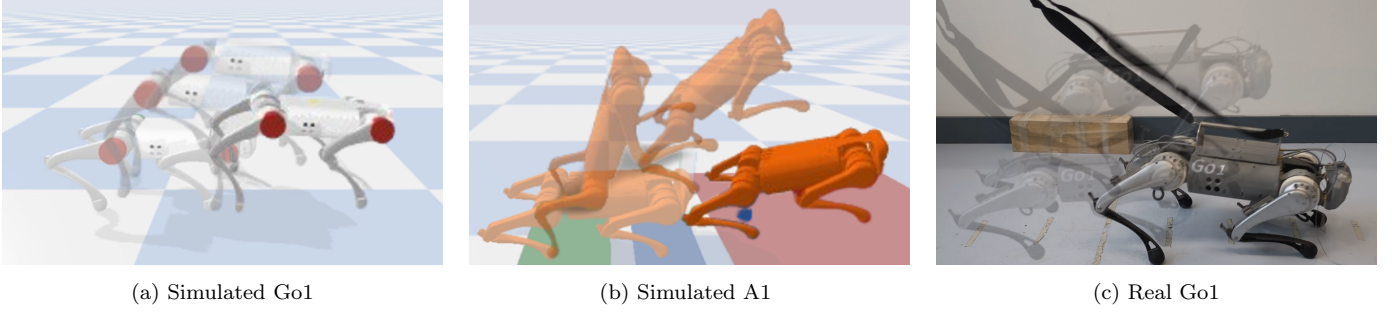


Fig. 4. A sequential images of quadruped jumps: (a) A simulated Go1 robot performs a vertically-oriented jump. (b) A simulated A1 executes a froggy jump. (c) A Go1 robot performs a (vertically-oriented) jump in the real world.

tion over time, showcasing the precision of the model for medium-horizon forecasts, as it would be used in planning and control frameworks such as MPC.

In this study, we regard the aSLIP model (see Appendix.A) as the baseline for predicting the dynamical behavior.

4. RESULTS

This section evaluates the approach using simulated Unitree Go1 and A1 quadrupeds data and real-world data from a Unitree Go1.

4.1 Go1 Simulation Results

Learning in 2D Latent Space for Go1 We initially explored a two-dimensional latent model for the synchronized jumping. Fig. 5 visualizes the transposed weight matrix \mathbf{W}_e^T of the trained encoder, indicating that the (learned) latent dimensions primarily correspond to the robot’s body center positions in the x and z coordinates.

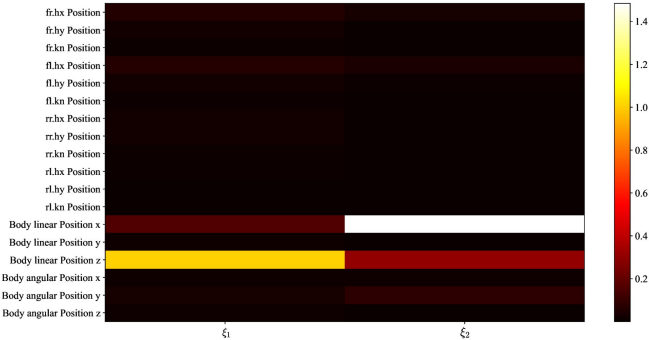


Fig. 5. Heatmap of the encoder’s transposed weight matrix \mathbf{W}_e^T trained on the simulated Go1 dataset with two latent dimensions. Brighter colors indicate higher absolute weights. The vertical axis shows the 18 configuration dimensions, and the horizontal axis shows the two latent dimensions.

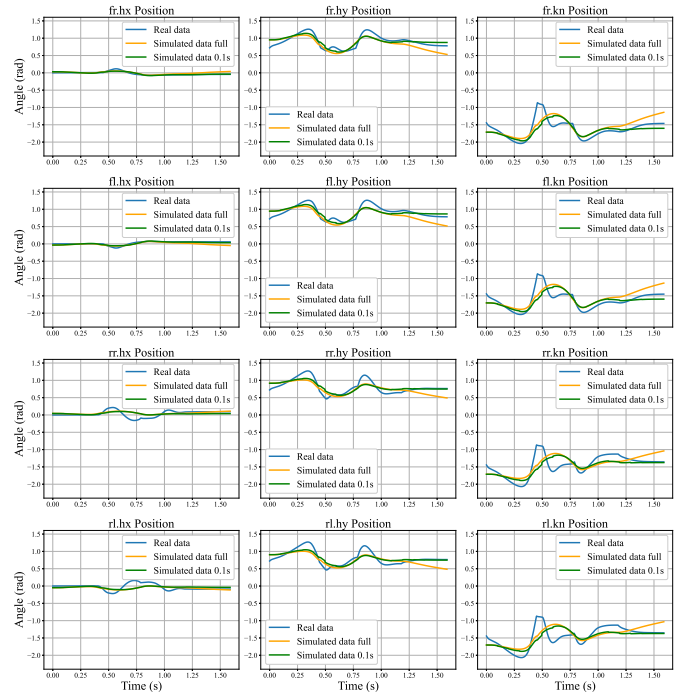
The learned equations of motion in the latent space for the contact and flight phases, respectively, are

$$\begin{cases} \ddot{\xi}_1 = 0.36 - 0.16 \dot{\xi}_1 - 0.91 \dot{\xi}_2 - 0.75 \sin(\dot{\xi}_1) + 0.11 \nu_1 - 0.05 \nu_2 \\ \ddot{\xi}_2 = -0.16 - 0.23 \dot{\xi}_1 - 0.75 \dot{\xi}_2 - 0.96 \sin(\dot{\xi}_2) + 0.14 \nu_2 \end{cases}, \quad (12)$$

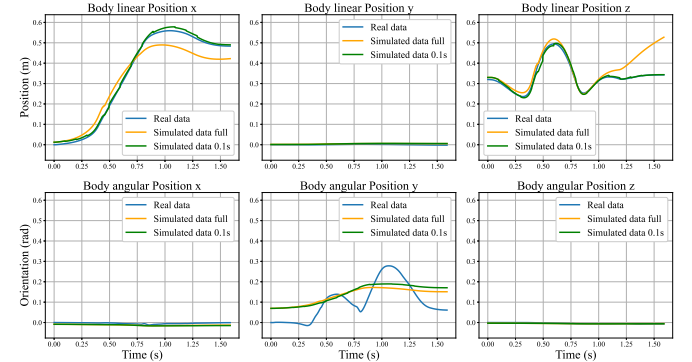
and

$$\begin{cases} \ddot{\xi}_1 = 0.29 - 1.22 \dot{\xi}_1 - 1.00 \sin(\dot{\xi}_1) + 51.05 \nu_1 \\ \ddot{\xi}_2 = 0.42 \dot{\xi}_1 + 0.52 \sin(\dot{\xi}_1) \end{cases}. \quad (13)$$

The prediction results for simulated Go 1 jumping are shown in Fig. 6.



(a) Joint angles (Joint notations are detailed in Fig. 1)



(b) CoM positions and orientations

Fig. 6. Evaluation of the trained model with two latent dimensions on the simulated Go1 jumping dataset.

Fig. 7 compares the body’s linear position along the x and z axes, demonstrating that the learned model outperforms, especially in the x axis, the baseline aSLIP model.

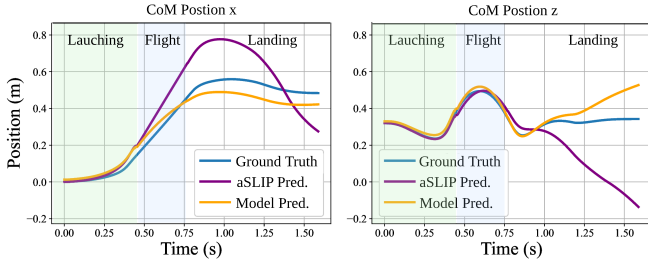


Fig. 7. Comparison between the learned model and the aSLIP model, on the task of predicting the CoM linear positions along the x and z axes, where the simulated Go 1 performs a jumping motion.

Latent Space Dimensionality Tradeoff Analysis We analyze the effect of latent dimensionality on model design. As shown in Fig. 8, increasing to 18 dimensions does not change the dominance of key full-order components. Fig.9 further evaluates the trade-off between accuracy (via

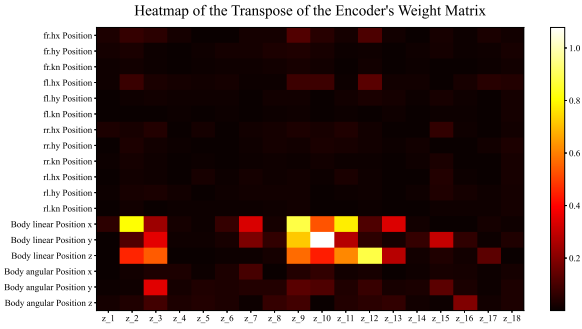


Fig. 8. Heatmap visualization of the transposed weight matrix \mathbf{W}_e^T of the encoder trained on the simulated Go1 dataset in the case of 18 latent dimensions.

final reconstruction error \mathcal{E}_{dec} and complexity (via active SINDy coefficients $|\Xi|$) across 18 contact phase models with varying latent dimensions.

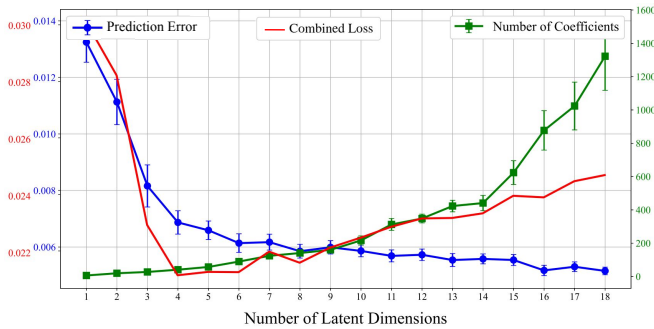
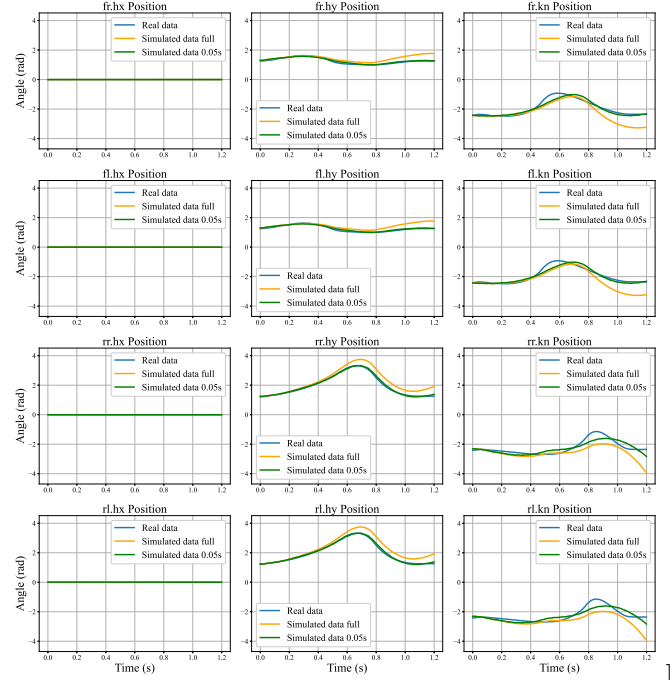
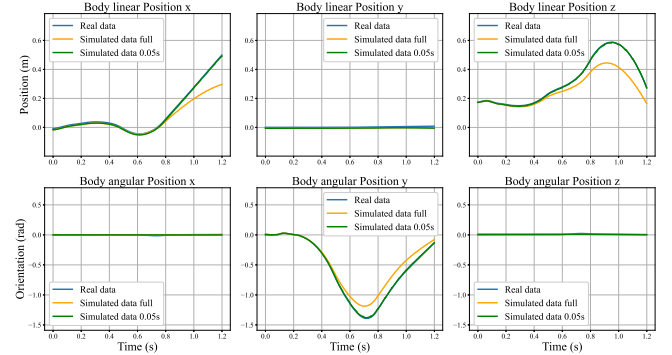


Fig. 9. The trade-off between accuracy and complexity with increasing latent dimensions evaluated on the simulated Go1 dataset. The error bars depict the standard deviation from five different random seeds.



(a) Joint angles



(b) CoM positions and orientations

Fig. 10. Evaluation of the proposed method with four latent dimensions on A1 froggy jumping.

To quantitatively evaluate this trade-off, we employ a combined loss \mathcal{L}_{mod} that is inspired by the Akaike Information Criterion (AIC) for model selection (Bozdogan, 1987) and calculated as

$$\mathcal{L}_{\text{mod}} = 2\mathcal{E}_{\text{dec}} + 2\lambda \log(|\Xi|), \quad (14)$$

with $\lambda = 0.001$, balancing the loss terms, the combined loss (red line in Fig.9) suggests optimal performance with 4–6 latent dimensions. This aligns with the visibly significant components in Fig.8, where further increasing dimensionality yields marginal gains at the cost of complexity.

4.2 A1 Simulation Results

We also conducted experiments on data collected with a simulated Unitree A1 quadruped executing a froggy jump to evaluate the algorithm’s effectiveness across different platforms. The results are illustrated in Fig. 10. A notable difference is observed in the body angular position y between the Unitree A1 and the Unitree Go1. The froggy jump causes a more pronounced angular rotation along the

5. DISCUSSION AND CONCLUSION

The results of our symbolic learning framework show that a reduced latent space can effectively preserve key dynamic patterns of the quadruped robot jumping motion. By combining autoencoder-based embeddings with sparse regression, we obtain interpretable and compact models that approximate the complex full-order dynamics. Our analysis of latent dimensionality shows that increasing beyond 4–6 dimensions offers diminishing returns in accuracy while introducing additional model complexity. The sim-to-real transfer results indicate that the model retains core dynamic features and generalizes well despite limited real-world data, validating its robustness to measurement noise and domain shift.

In future work, we aim to extend this methodology to more dynamic behaviors, such as walking and running, and to systems involving rapid contact changes or higher-dimensional morphologies, including humanoids.

REFERENCES

- Bellicoso, C.D., Jenelten, F., Fankhauser, P., Gehring, C., Hwangbo, J., and Hutter, M. (2017). Dynamic locomotion and whole-body control for quadrupedal robots. In *2017 IEEE/RSJ International Conference on Intelligent Robots and Systems (IROS)*, 3359–3365. IEEE.
- Blickhan, R. (1989). The spring-mass model for running and hopping. *Journal of biomechanics*, 22(11-12), 1217–1227.
- Bozdogan, H. (1987). Model selection and akaike’s information criterion (aic): The general theory and its analytical extensions. *Psychometrika*, 52(3), 345–370.
- Brunton, S.L., Proctor, J.L., and Kutz, J.N. (2016). Discovering governing equations from data by sparse identification of nonlinear dynamical systems. *Proceedings of the national academy of sciences*, 113(15), 3932–3937.
- Calandra, R., Ivaldi, S., Deisenroth, M.P., Rueckert, E., and Peters, J. (2015). Learning inverse dynamics models with contacts. In *2015 IEEE International Conference on Robotics and Automation (ICRA)*, 3186–3191. IEEE.
- Carpentier, J. and Mansard, N. (2018). Multicontact locomotion of legged robots. *IEEE Transactions on Robotics*, 34(6), 1441–1460.
- Champion, K., Lusch, B., Kutz, J.N., and Brunton, S.L. (2019). Data-driven discovery of coordinates and governing equations. *Proceedings of the National Academy of Sciences*, 116(45), 22445–22451.
- Coumans, E. and Bai, Y. (2016). Pybullet, a python module for physics simulation for games, robotics and machine learning.
- Di Carlo, J., Wensing, P.M., Katz, B., Bledt, G., and Kim, S. (2018). Dynamic locomotion in the mit cheetah 3 through convex model-predictive control. In *2018 IEEE/RSJ international conference on intelligent robots and systems (IROS)*, 1–9. IEEE.
- Ding, J., Atanassov, V., Panichi, E., Kober, J., and Della Santina, C. (2024a). Robust quadrupedal jumping with impact-aware landing: Exploiting parallel elasticity. *IEEE Transactions on Robotics*, 40, 3212–3231.
- Ding, J., Posthoorn, P., Atanassov, V., Boekel, F., Kober, J., and Della Santina, C. (2024b). Quadrupedal locomotion with parallel compliance: E-go design, modeling,

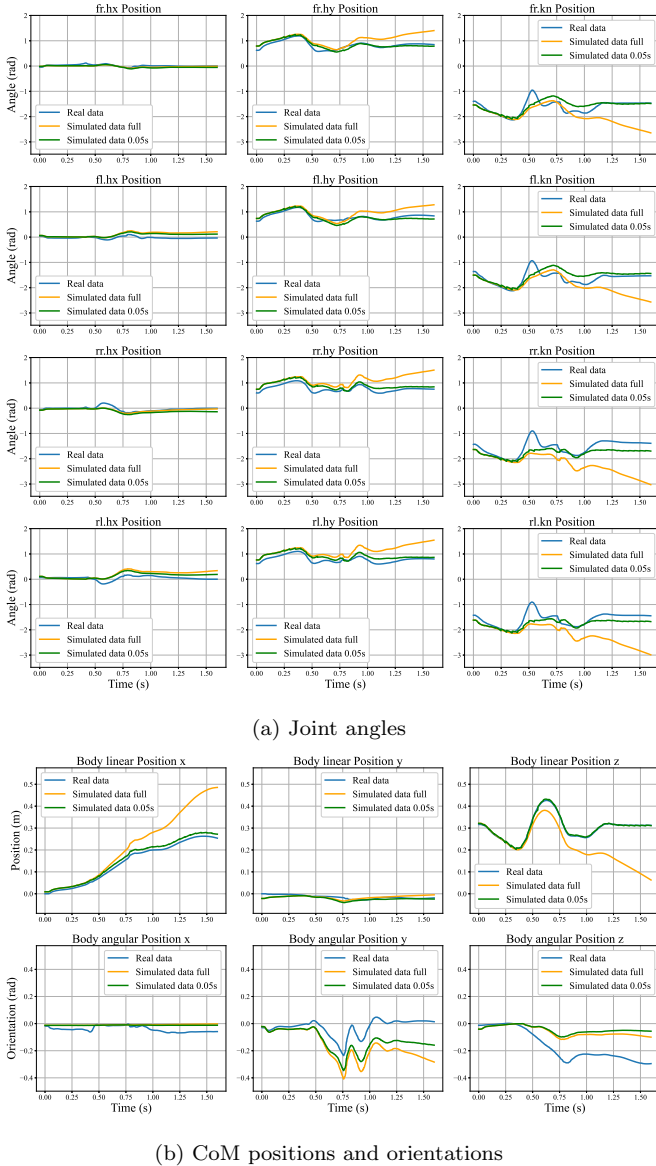


Fig. 11. Evaluation of the learned reduced-order model with four latent dimensions on the Go1 real-world testing dataset.

y -axis in the A1’s case. Despite the increased significance of this angular dimension for the jump motion, the four-dimensional model successfully captures this dynamic and most joint positions.

4.3 Go1 Real World Results

Given the scarcity of real-world compared to simulated data, we first train the model on simulation data with added noise and then subsequently fine-tune it on the few-sample real-world dataset. Fig. 11 illustrates the model’s ability to replicate a jump on the hardware, comparing joint angles and CoM positions and orientations.

The proposed model performs well on actual hardware data, despite reduced accuracy during flight and initial landing phases compared to simulations. Nonetheless, the model effectively manages real-world noise and complexity, demonstrating robust performance.

- and control. *IEEE/ASME Transactions on Mechatronics*, 29(4), 2839–2848.
- Gong, Y., Sun, G., Nair, A., Bidwai, A., CS, R., Grezma, J., Sartoretto, G., and Daltorio, K.A. (2023). Legged robots for object manipulation: A review. *Frontiers in Mechanical Engineering*, 9, 1142421.
- Gonzalez, F.J. and Balajewicz, M. (2018). Deep convolutional recurrent autoencoders for learning low-dimensional feature dynamics of fluid systems. *arXiv preprint arXiv:1808.01346*.
- Hashemi, A., Orzechowski, G., Mikkola, A., and McPhee, J. (2023). Multibody dynamics and control using machine learning. *Multibody System Dynamics*, 58(3), 397–431.
- Hindmarsh, A.C. and Petzold, L.R. (2005). Lsodar, ordinary differential equation solver for stiff or non-stiff system with root-finding.
- Hinton, G.E. and Salakhutdinov, R.R. (2006). Reducing the dimensionality of data with neural networks. *science*, 313(5786), 504–507.
- Hong, S., Kim, J.H., and Park, H.W. (2020). Real-time constrained nonlinear model predictive control on so (3) for dynamic legged locomotion. In *2020 IEEE/RSJ International Conference on Intelligent Robots and Systems (IROS)*, 3982–3989. IEEE.
- Li, J., Gao, H., Wan, Y., Yu, H., and Zhou, C. (2023). A real-time planning and control framework for robust and dynamic quadrupedal locomotion. *Journal of Bionic Engineering*, 20(4), 1449–1466.
- Liu, J., Borja, P., and Della Santina, C. (2024). Physics-informed neural networks to model and control robots: A theoretical and experimental investigation. *Advanced Intelligent Systems*, 6(5), 2300385.
- Lutter, M., Ritter, C., and Peters, J. (2019). Deep lagrangian networks: Using physics as model prior for deep learning. *arXiv preprint arXiv:1907.04490*.
- Mistry, M., Buchli, J., and Schaal, S. (2010). Inverse dynamics control of floating base systems using orthogonal decomposition. In *2010 IEEE international conference on robotics and automation*, 3406–3412. IEEE.
- Nguyen, C. and Nguyen, Q. (2022). Contact-timing and trajectory optimization for 3d jumping on quadruped robots. In *2022 IEEE/RSJ international conference on intelligent robots and systems (IROS)*, 11994–11999. IEEE.
- Ogunmolu, O., Gu, X., Jiang, S., and Gans, N. (2016). Nonlinear systems identification using deep dynamic neural networks. *arXiv preprint arXiv:1610.01439*.
- Pandey, P., Khodaparast, H.H., Friswell, M., Chatterjee, T., Jamia, N., and Deighan, T. (2024). Data-driven system identification of unknown systems utilising sparse identification of nonlinear dynamics (sindy). In *Journal of Physics: Conference Series*, volume 2647, 062006. IOP Publishing.
- Raissi, M., Perdikaris, P., and Karniadakis, G.E. (2019). Physics-informed neural networks: A deep learning framework for solving forward and inverse problems involving nonlinear partial differential equations. *Journal of Computational physics*, 378, 686–707.
- Rajendra, P. and Brahmajirao, V. (2020). Modeling of dynamical systems through deep learning. *Biophysical Reviews*, 12(6), 1311–1320.
- Refinetti, M. and Goldt, S. (2022). The dynamics of representation learning in shallow, non-linear autoencoders. In *International Conference on Machine Learning*, 18499–18519. PMLR.
- Righetti, L., Buchli, J., Mistry, M., and Schaal, S. (2011). Inverse dynamics control of floating-base robots with external constraints: A unified view. In *2011 IEEE international conference on robotics and automation*, 1085–1090. IEEE.
- Sombolestan, M. and Nguyen, Q. (2024). Adaptive-force-based control of dynamic legged locomotion over uneven terrain. *IEEE Transactions on Robotics*, 40, 2462–2477.
- Spröwitz, A., Tuleu, A., Vespignani, M., Ajallooeian, M., Badri, E., and Ijspeert, A.J. (2013). Towards dynamic trot gait locomotion: Design, control, and experiments with cheetah-cub, a compliant quadruped robot. *The International Journal of Robotics Research*, 32(8), 932–950.
- Stölzle, M. (2025). *Safe yet Precise Soft Robots: Incorporating Physics into Learned Models for Control*. Dissertation (tu delft), Mechanical Engineering, Delft University of Technology.
- Stölzle, M. and Santina, C.D. (2024). Input-to-state stable coupled oscillator networks for closed-form model-based control in latent space. In *Proceedings of the 38th International Conference on Neural Information Processing Systems*, 82010–82059.
- Torrey, L. and Shavlik, J. (2010). Transfer learning. In *Handbook of research on machine learning applications and trends: algorithms, methods, and techniques*, 242–264. IGI Global Scientific Publishing.
- Yan, W., Pan, Y., Che, J., Yu, J., and Han, Z. (2021). Whole-body kinematic and dynamic modeling for quadruped robot under different gaits and mechanism topologies. *PeerJ Computer Science*, 7, e821.

Appendix A. BASELINE: ACTUATED SLIP MODEL

The actuated SLIP (aSLIP) (Ding et al., 2024a) model extends the basic SLIP model by incorporating actuators, allows for enhanced control over legged jumping, as depicted in Fig. A.1. The CoM acceleration $\ddot{\mathbf{b}}$ is

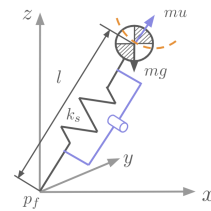


Fig. A.1. The aSLIP model. The actuation (denoted as $\mu\mathbf{u}$) is explicitly captured to enhance controllability.

$$\begin{aligned} \text{In flight: } \ddot{\mathbf{b}} &= \mathbf{g} \\ \text{In Contact: } \ddot{\mathbf{b}} &= \frac{k_s|\mathbf{l}_0 - \mathbf{l}|\hat{\mathbf{l}}}{m} + \mathbf{g} + \mathbf{u} \end{aligned} \quad (\text{A.1})$$

where $k_s \in \mathbb{R}^+$ is the spring constant, $m \in \mathbb{R}^+$ is the body mass, $\mathbf{l} = \mathbf{b} - \mathbf{p}_k$ is the leg vector, $\hat{\mathbf{l}}$ is the unit vector along the leg retraction direction, \mathbf{l}_0 is the rest length, and $\mathbf{g} = [0, 0, -g]^\top$ with g being the vertical gravitational constant. $\mathbf{u} \in \mathbb{R}^3$ are the driving forces generated by joint motors, which can be seen as the accumulated GRFs on four legs, as calculated using (3).